Theory of Quantum Anomalous Hall Phases in Pentalayer Rhombohedral Graphene Moiré Structures

Zhihuan Dong,* Adarsh S. Patri,* and T. Senthil
Department of Physics, Massachusetts Institute of Technology, Cambridge, Massachusetts 02139, USA

(Received 19 November 2023; accepted 26 August 2024; published 12 November 2024)

Remarkable recent experiments on the moiré structure formed by pentalayer rhombohedral graphene aligned with a hexagonal boron nitride substrate report the discovery of a zero field fractional quantum Hall effect. These "(fractional) quantum anomalous Hall" [(F)QAH] phases occur for one sign of a perpendicular displacement field, and correspond, experimentally, to full or partial filling of a valley polarized Chern-1 band. Such a band is absent in the noninteracting band structure. Here we show that electron-electron interactions play a crucial role, and present microscopic theoretical calculations demonstrating the emergence of a nearly flat, isolated, Chern-1 band and FQAH phases in this system. We also study the four- and six-layer analogs and identify parameters where a nearly flat isolated Chern-1 band emerges which may be suitable to host FQAH physics.

DOI: 10.1103/PhysRevLett.133.206502

Recent experiments have observed [1–5] the fractional quantum Hall effect in systems that microscopically are time-reversal invariant. The corresponding states of matter —known as fractional quantum qnomalous Hall (FQAH) phases—break time reversal spontaneously. FQAH states were first evidenced in twisted $MoTe_2$ moiré heterostructures through measurements of the location of the many-body gap [1,2] as a function of density and magnetic field, and subsequently, in transport [3,4].

Very recently, many FQAH states have been discovered [5] in pentalayer rhombohedral graphene aligned with a hexagonal boron nitride (h-BN) substrate. We show, through microscopic calculations, in this Letter that these arise due to a novel mechanism where Coulomb interactions stabilize a nearly flat isolated Chern band which then sets the stage for the appearance of FQAH physics.

Rhombohedral graphene refers to a structure where different layers of graphene are stacked together in the ABC pattern shown in Fig. 1(a). Without the h-BN alignment, a first-cut description of the band structure, when there are a total of n such layers, is that valence and conduction bands have a very flat nth order band touching (with a k^n dispersion where k is the wave number) in each of the two valleys. A more accurate band structure, shown in Fig. 1(b), that includes the effects of trigonal warping modifies the precise high-order band touching. The flatness of the bands near neutrality enhances the effects of Coulomb interaction, as evidenced by the discovery [6–12], in the last few years, of interaction-driven many-body states in $n = 2$, 3, 4, 5 rhombohedral graphene. We will denote n-layer rhombohedral graphene as RnG below; if it is further aligned with h-BN on one side we denote it as RnG/h-BN.

In RnG/h-BN the slight lattice mismatch between graphene and h-BN produces a moiré pattern which strongly modifies the electronic band structure [13]. Theoretical study [14] of R3G/h-BN showed that the moiré bands are nearly flat. Further, the band structure is very sensitive [14] to a perpendicular displacement field D. For one sign of the displacement field, the bands are topological with valley Chern number ± 3, while for the other sign, they have Chern number 0. The topological side occurs when the active change carriers are driven away from the aligned layer. These features lead to the proposal [14] that these systems will, for one sign of D, be good platforms to obtain (fractional) quantum anomalous Hall effects with the requisite time-reversal breaking realized

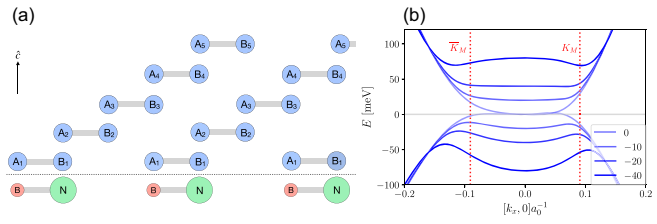

FIG. 1. (a) Schematic of pentalayer rhombohedral graphene (R5G), with and without aligned h-BN on layer 1. Carbon atoms highlighted in blue, boron atoms in red, and nitrogen atoms in green. The alignment is chosen here so that A_1 (B_1) aligns with boron (nitrogen). (b) Continuum R5G dispersion (without h-BN alignment) along the k_x axis for increasing interlayer potential difference u_d (meV) highlighted by darker shades of blue. The vertical dashed lines indicate the location of the moiré K points when h-BN is aligned with pentalayer graphene.

*These authors contributed equally to this work.

through valley (and spin) polarization. Indeed, experiments [15] on R3G/h-BN at total filling $\nu_T = 1$ of the valence band observe an integer quantum anomalous Hall state with a Chern number 2. The change of Chern number to 2 from the naive band theory expectation of 3 was explained [15] through a Hartree-Fock calculation that includes mixing with the next remote band.

Generalized to RnG/h-BN, the naive expectation is that for one sign of D, the bands will have a valley Chern number $\pm n$, and hence might show an integer quantum anomalous Hall effect with $\sigma_{xy} = \pm(ne^2/h)$ at total odd-integer filling of the moiré bands. However, the experiments of Ref. [5] on R5G/h-BN see an integer quantum Hall effect with $\sigma_{xy} = \pm(e^2/h)$ at $\nu_T = 1$ of the conduction band. Further, the FQAH states observed at fractional filling ($\nu_T = 2/3, 3/5, \ldots$) are what might be expected at partial fractional filling of a Chern-1 band. The theoretical noninteracting band structure (at the large displacement field energies corresponding to those in Ref. [5]) is shown in Fig. 3, and does not even have an isolated conduction band, let alone a Chern number. Thus a task for theory is to first explain the emergence of an isolated Chern-1 band in the R5G/h-BN system and next to demonstrate that this Chern band hosts FQAH phases.

Here, we present a Hartree-Fock treatment of the band structure in the presence of both an aligned h-BN substrate as well as a perpendicular displacement field. We identify a range of displacement fields where there is an interaction-induced first conduction band (see Fig. 2) that is isolated from other bands, has a small bandwidth, and a net Chern number of ± 1 in each of the two graphene valleys. We provide evidence of valley polarization consistent with experiments. At partial rational fillings of the valley polarized bands, we then show using exact diagonalization studies that FQAH phases develop. Our results provide a microscopic basis for the observation of FQAH physics in R5G/h-BN. We also explore the renormalized band structure of RnG/h-BN, for $n = 4$, 6, finding parameters with nearly flat Chern-1 bands that are well separated from other bands. Thus R4G/h-BN and R6G/h-BN may also be good platforms for FQAH physics.

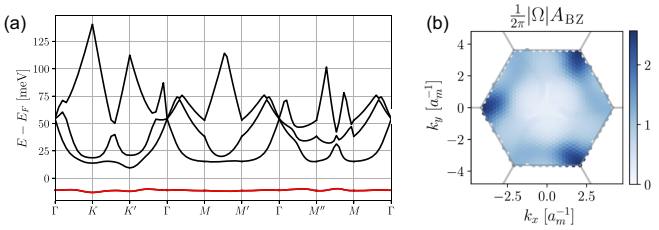

FIG. 2. (a) Hartree-Fock band structure of R5G/h-BN for a single valley with an interlayer potential difference $u_d = -36$ meV, and relative dielectric constant $\epsilon = 8$, and (b) Berry curvature Ω multiplied by the moiré Brillouin zone area A_{BZ}. The active conduction band (highlighted in red) is flat (bandwidth of 4 meV), well separated from the remote conduction bands above (direct gap of 19 meV and global gap of 17 meV), and carries a Chern number $|C| = 1$. Momentum mesh of 30×30, and keeping the four lowest conduction bands.

The importance of electronic interactions in obtaining the nearly flat isolated Chern band in RnG/h-BN makes them unique compared to the theory of previously explored platforms [16–27] or of toy models [28–36].

Model of R5G/h-BN—In R5G, for a given spin and valley, there are 2 sublattice degrees of freedom per layer, leading to a description of the noninteracting physics in terms of a 10-band model. A perpendicular displacement field implies a potential difference between adjacent layers (denoted u_d). The resulting tight-binding model is described in Supplemental Material (SM) Sec. I [37]. At low energies near the charge neutrality point, the important degrees of freedom lie in one sublattice (say the A sublattice) in the bottom layer and in the opposite B sublattice in the top layer. A displacement field tends to drive electrons preferentially to either the top or bottom layer depending on its sign.

The R5G is subjected to an underlying moiré potential through the (near) alignment of one end, which we take to be the bottom layer, with an h-BN substrate. We choose an alignment angle of 0.77° to match the angle quoted in Ref. [5]. The moiré potential is modeled as

$$H_M = \sum_{\mathbf{G}} c_1^\dagger(\mathbf{k}+\mathbf{G}) V_M(\mathbf{G}) c_1(\mathbf{k}), \tag{1}$$

where $V_M(\mathbf{G})$ is defined in SM Sec. I [37], and $\mathbf{G}$ are the reciprocal lattice vectors of the moiré superlattice.

To discuss many-body physics, we take a dual gate-screened Coulomb interaction between the low-energy electrons,

$$H_C = \frac{1}{2A} \sum_{\mathbf{k},\mathbf{k}',\mathbf{q}} \sum_{\mu,\nu} V_C^{\mathrm{sc}}(\mathbf{q}) c^\dagger_{\mathbf{k}+\mathbf{q};\mu} c^\dagger_{\mathbf{k}'-\mathbf{q};\nu} c_{\mathbf{k}';\nu} c_{\mathbf{k};\mu}, \tag{2}$$

where A is the area of the system, μ, ν denotes a compact sublattice-valley-flavor index, $V_C^{\mathrm{sc}}(\mathbf{q}) = (e^2/2\epsilon_0\epsilon q)\tanh(qd_s)$ is the screened potential, ϵ is the effective dielectric constant, and d_s is the distance between the metallic gates and the top and bottom layers (taken to be 30 nm).

We begin with the noninteracting band structure in the moiré Brillouin zone. Figure 1(b) shows the continuum dispersion for one valley of isolated R5G for increasing displacement field energies $u_d < 0$. The sign of u_d is such that electrons are driven away from the aligned h-BN. For $u_d = 0$, there is a band touching at the Γ point. As the magnitude of the displacement field energy is increased, a band gap develops in conjunction with a flattening of the conduction band.

When subjected to an aligned moiré potential, the continuum band reconstructs into the moiré Brillouin zone.

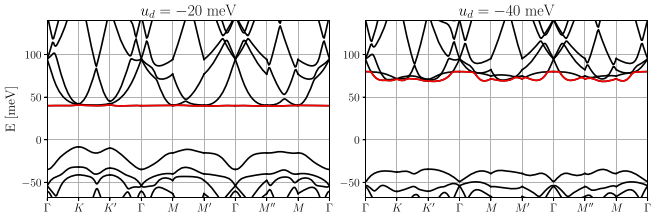

FIG. 3. Noninteracting band structure for R5G/h-BN for displacement field energies $u_d = -20, -40$ meV. There is a wide gap between valence and conduction bands.

The moiré K point is at $\approx 0.1/a_0$; as seen in Fig. 1(b) this corresponds to the low-energy conduction moiré bands being formed predominantly by the "flat" region of the conduction continuum band. Figure 3 shows the moiré band structure for displacement fields of $u_d = -20, -40$ meV. With increasing displacement field, the active conduction band (highlighted in red) separates away from the valence bands but eventually collides with the higher "remote" conduction bands for $u_d \gtrsim -40$ meV. Thus for a large displacement field, we expect that interaction effects will mix together various conduction bands, and lead to a renormalized band structure with modified Bloch functions, and possibly, open up a band gap.

Hartree-Fock interaction effects for R5G/h-BN—To deal with these effects, we perform a Hartree-Fock calculation (see SM Sec. II [37]) of the band structure in a single valley (and ignoring electron spin) keeping the first three conduction bands. We present in Fig. 2 the renormalized band structure and the Berry curvature Ω. The band is very flat (bandwidth of ≈ 4 meV), with a global gap to the neighboring conduction band of ≈ 17 meV. Moreover, the Berry curvature has redistributed to make the band have $|C| = 1$. We emphasize that both the band gap and the Chern number are interaction-induced and are absent in the free-electron band structure.

Figure 4 shows the Hartree-Fock band structure "phase diagram" as the displacement field and dielectric constant are swept over a range of parameters. There is a stripe in parameter space of obtaining $|C| = 1$ band that is conducive to forming a correlated state, i.e., has a narrow bandwidth and a well-separated gap from the other bands. Indeed, there is an optimal window (i.e., minimum bandwidth and maximum gap) for $|u_d| \approx 35$–40 meV and $\epsilon \approx 5$–10. The prevalence of the Chern band (over the topologically trivial band) can be heuristically understood as a consequence of the Wannier obstruction of topological bands: the prohibition of exponentially localized real-space wave functions leads to a more evenly distributed charge density, thereby reducing the Coulomb repulsion.

To further characterize the renormalized band structure in Fig. 5, we show the quantum metric g_{ij}, and the quantity $T = (A_{\mathrm{BZ}}/2\pi)\int_{\mathrm{BZ}} d^2k\,\mathrm{tr}(g) - |\Omega|$, where A_{BZ} is the area of the Brillouin zone. For an "ideal" Chern band [36,43,44]

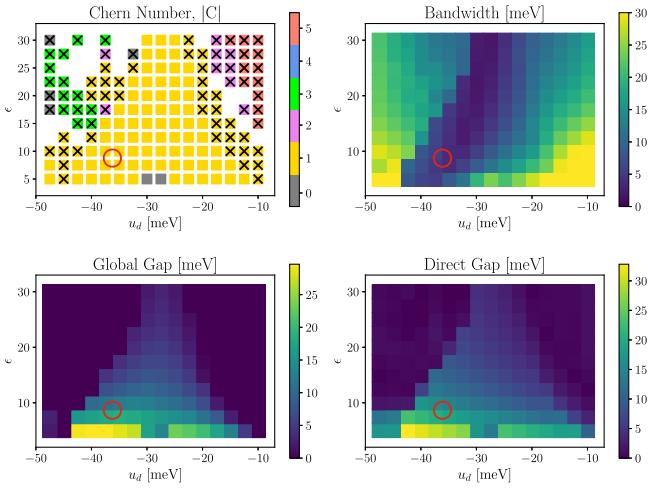

FIG. 4. Hartree-Fock bands indicating Chern number and bandwidth of the active band, global band gap, and direct band gap to nearest conduction band for different displacement field energies u_d and dielectric constant ϵ. The Chern number is well defined when the direct band gap is nonzero (≥ 0.5 meV). The "crossed" out yellow boxes in the Chern number indicate cases where the global band gap is zero (< 0.5 meV), while the direct band gap is still nonzero (i.e., there is an indirect band gap—the system is metallic). Phase diagrams are for a mesh of 27×27 and constructed using 19 moiré Brillouin zones, and generated using at least five distinct initial mean-field *Ansätze* for a given parameter point. The red-circled region is the parameter chosen for the exact diagonalization (ED).

$T = 0$. Intriguingly, the $|C| = 1$ conduction band has an average trace violation of $\langle T \rangle \approx 0.9$; for comparison, for the first Landau Level this violation is 2.

In Fig. 5, we also show the occupation numbers in the top layer and the layer directly underneath it. At these large displacement fields, the electrons mostly reside just in the top layer (with some small charge density in the adjacent layer below).

R5G/h-BN has four flavor degrees of freedom (spin and valley). Spontaneous valley polarization breaks time-reversal symmetry and enables the electrons to have a net nonzero Chern number. If, in addition, the spin is also polarized, then the many-body state at total filling $\nu_T = 1$ will be an integer quantum anomalous Hall (IQAH) state. This is the mechanism [14,45–47] for the ferromagnetism [48] and the IQAH effect [15,49–51] observed in graphene moiré structures.

We present the Hartree-Fock band structure including both spin and valley degrees of freedom in Fig. 6. The lowest conduction band is fully spin-valley polarized. However the fate of the spin deserves more discussion. In the main text, we assume full spin polarization and relax this assumption in SM Sec. IV [37].

Evidence of FQAH from exact diagonalization—We now project (see SM Sec. II [37]) the Coulomb interaction to the active conduction Chern band and demonstrate that FQAH states emerge within an exact diagonalization study.

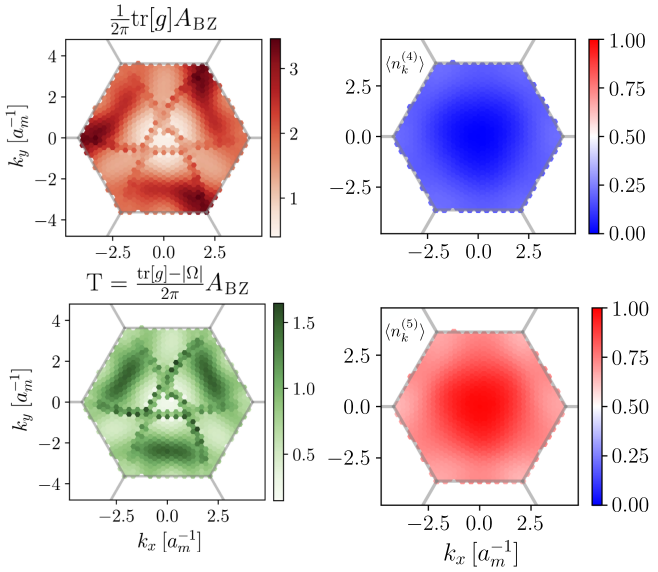

FIG. 5. Hartree-Fock determined quantum metric, and trace condition, accompanied by the layer-four, layer-five occupation number. The total weight on the other 3 layers combined is ≈5%. The mean and variance of the trace condition over the BZ is $\langle T\rangle = 0.9$ and $\mathrm{var}(T) = 0.09$, respectively.

We study the spectrum of the resulting many-body Hamiltonian in a torus geometry, as shown in Fig. 7(a) and Fig. A.2 in SM Sec. III [37]. We focus on band filling 2/3 here; data at other fillings are in SM Sec. III [37]. At 2/3 filling, there is a set of 3 nearly degenerate states that are well separated (and lower) in energy than other states, consistent with a FQAH state.

Next, we study the evolution of the spectrum upon inserting a single flux quantum through one cycle of the torus. In a FQAH state, this flux threading is equivalent to generating a quasihole and quasiparticle pair, moving one of them around one noncontractable loop of the torus, and annihilating the pair. This connects topologically distinct ground states on the torus. On a system with $N_x \times N_y$ geometry and at filling ν, flux threading of $\Delta\Phi$ leads to a many-body momentum shift of

$$\Delta k_i = \frac{\Delta\Phi_i}{L_i} L_x L_y \nu. \tag{3}$$

The momentum shift for the geometry and filling in Fig. 7(a) is consistent with this expectation.

The spectral flow under unit flux insertion is shown in Fig. 7(b). The 3 nearly degenerate ground states are permuted under the flux insertion, consistent with the FQAH state. Furthermore, these states remain well separated from the excited states at all values of the flux.

In Fig. 7(c), we demonstrate the particle entanglement spectrum (PES) [33,52], which encodes the information of the quasihole Hilbert space dimension. For this purpose, we partition the system into subsystems A and B, with N_A and N_B electrons and momentum k_A and k_B, respectively. The PES ξ_i is associated with the eigenvalue λ_i of reduced density matrix $\rho_B = \mathrm{Tr}_A\rho$ through $\xi_i = -\log\lambda_i$. For $\nu = 2/3$, the ground states are threefold degenerate, and we take $\rho = \frac{1}{3}(|\tilde{\Psi}_1\rangle\langle\tilde{\Psi}_1| + |\tilde{\Psi}_2\rangle\langle\tilde{\Psi}_2| + |\tilde{\Psi}_3\rangle\langle\tilde{\Psi}_3|)$, where $|\tilde{\Psi}_i\rangle = P|\Psi_i\rangle$ are the particle-hole conjugate of

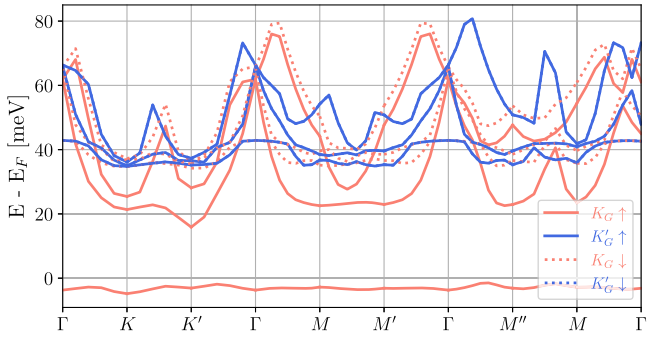

FIG. 6. Spin-valley polarization of Hartree-Fock band structure for displacement field $u_d = -36$ meV, and relative dielectric constant $\epsilon = 8$. The colors label two valleys, and the solid (dotted) lines indicate the spin orientation ↑ (↓). The active conduction band is polarized in the monolayer graphene valley $\{K_G, \uparrow\}$ throughout the Brillouin zone. The spin-valley polarization is spontaneously chosen (with a nonspontaneously chosen spin-polarization degeneracy remaining in the band structure). This calculation is performed on a momentum mesh of 15×15 and keeping the three lowest conduction bands.

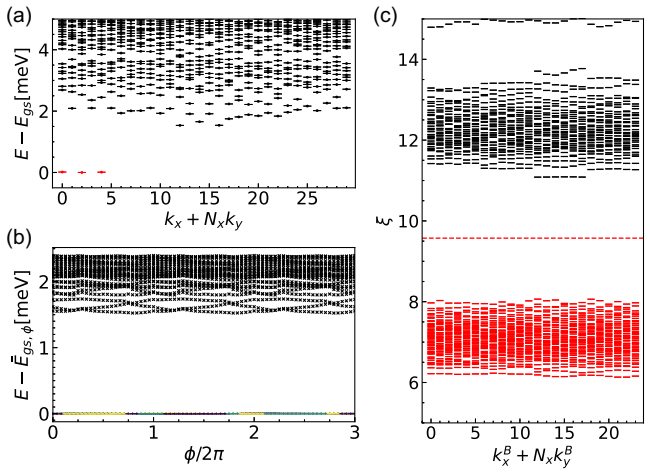

FIG. 7. Evidence for FQAH at $\nu = 2/3$ from exact diagonalization. (a) Low-energy spectrum of a spin-valley polarized system with $N_x \times N_y = 6 \times 5$. (b) Spectral flow under flux threading along x direction on 6×4 system. $\bar{E}_{\mathrm{g.s.}}$ is the average energy for topologically degenerate ground states. The colors are identified by the momentum sector corresponding to the eigenstates. (c) Particle entanglement spectrum (PES) for the particle-hole conjugate of $\nu = 2/3$ states. With a subsystem containing $N_B = 3$ holes on a 6×4 lattice, we find the total number of states below the gap is 1088, consistent with the expectation [33] for FQAH. These results are obtained at $\epsilon = 8$, $D = -36$ meV.

topologically degenerate ground states. The counting of states agrees exactly with that expected for the particle-hole conjugate of the $1/3$ Laughlin state (see also Fig. A.4(c) in SM Sec. IV [37]). Taken together our calculations strongly support the identification of the state at $2/3$ filling with an FQAH state. Other gapped states such as ones with charge density wave order are not compatible with these results.

In SM Sec. IV, we present calculations that do not assume spin polarization, and find a rich and nonmonotonic behavior as the filling is varied [37].

Discussion—An interesting question is the role of the moiré potential in the emergence of the isolated Chern-1 band. At $\nu = 1$, we checked that such a band emerges in Hartree-Fock even in the absence of moiré (SM Sec. VI [37]), consistent with Refs. [53,54]. This suggests a picture of the $\nu = 1$ state as a "Hall crystal" [55] weakly pinned by the moiré potential that should be examined beyond the Hartree-Fock approximation. As we emphasize elsewhere, it is likely that the role of moiré is to stabilize the Hall crystal relative to a correlated Fermi liquid; our calculations should be viewed as a description of this moiré -enabled Hall crystal [56]. Finally, we discuss the prospect of FQAH physics in other RnG/h-BN systems. In SM Secs. VII and VIII [37], we study the renormalized band structures of R4G/h-BN and R6G/h-BN for a single valley and spin within Hartree-Fock theory as a function of displacement field energy and dielectric constant. For concreteness, we take the same alignment angle with h-BN as in our studies of R5G/h-BN. For both R4G/h-BN and R6G/h-BN, we find parameter regimes where there is a well-isolated nearly flat Chern-1 band, and with quantum geometry comparable to that in R5G/h-BN. This agrees with the expectation that since at large displacement fields only the top two layers away from the h-BN have any occupation at all, the total number of layers does not matter much. However, the optimal range of the displacement field decreases with increasing n, consistent with the expectation that the bands are flatter for larger n. In all these systems, the physics is sensitive to the alignment angle with h-BN. We thus anticipate a rich and interesting phase diagram to be unearthed in RnG/h-BN as more of the parameter space is explored experimentally.

Note added—Recently, Refs. [53,54] with closely related, and consistent, results also appeared. Following these works, the stability of the AHC was examined in Refs. [56,57].

Acknowledgments—We thank Long Ju, Tonghang Han, and Zhengguang Lu for discussions of their experimental data, Cécile Repellin for sharing her insights on exact diagonalization studies of quantum Hall states, and Ya-Hui Zhang for many inspiring conversations and previous collaborations. T. S. was supported by NSF Grant No. DMR-2206305, and partially through a Simons Investigator Award from the Simons Foundation. This work was also partly supported by the Simons Collaboration on Ultra-Quantum Matter, which is a grant from the Simons Foundation (Grant No. 651446, T. S.). The authors acknowledge the MIT SuperCloud and Lincoln Laboratory Supercomputing Center for providing HPC resources that have contributed to the research results reported within this Letter.

[1] J. Cai, E. Anderson, C. Wang, X. Zhang, X. Liu, W. Holtzmann, Y. Zhang, F. Fan, T. Taniguchi, K. Watanabe, Y. Ran, T. Cao, L. Fu, D. Xiao, W. Yao, and X. Xu, Nature (London) **622**, 63 (2023).

[2] Y. Zeng, Z. Xia, K. Kang, J. Zhu, P. Knüppel, C. Vaswani, K. Watanabe, T. Taniguchi, K. F. Mak, and J. Shan, Nature (London) **622**, 69 (2023).

[3] H. Park, J. Cai, E. Anderson, Y. Zhang, J. Zhu, X. Liu, C. Wang, W. Holtzmann, C. Hu, Z. Liu, T. Taniguchi, K. Watanabe, J.-h. Chu, T. Cao, L. Fu, W. Yao, C.-Z. Chang, D. Cobden, D. Xiao, and X. Xu, Nature (London) **622**, 74 (2023).

[4] F. Xu, Z. Sun, T. Jia, C. Liu, C. Xu, C. Li, Y. Gu, K. Watanabe, T. Taniguchi, B. Tong, J. Jia, Z. Shi, S. Jiang, Y. Zhang, X. Liu, and T. Li, Phys. Rev. X **13**, 031037 (2023).

[5] Z. Lu, T. Han, Y. Yao, A. P. Reddy, J. Yang, J. Seo, K. Watanabe, T. Taniguchi, L. Fu, and L. Ju, Nature (London) **626**, 759 (2024).

[6] H. Zhou, T. Xie, A. Ghazaryan, T. Holder, J. R. Ehrets, E. M. Spanton, T. Taniguchi, K. Watanabe, E. Berg, M. Serbyn *et al.*, Nature (London) **598**, 429 (2021).

[7] H. Zhou, T. Xie, T. Taniguchi, K. Watanabe, and A. F. Young, Nature (London) **598**, 434 (2021).

[8] H. Zhou, L. Holleis, Y. Saito, L. Cohen, W. Huynh, C. L. Patterson, F. Yang, T. Taniguchi, K. Watanabe, and A. F. Young, Science **375**, 774 (2022).

[9] S. C. de la Barrera, S. Aronson, Z. Zheng, K. Watanabe, T. Taniguchi, Q. Ma, P. Jarillo-Herrero, and R. Ashoori, Nat. Phys. **18**, 771 (2022).

[10] Y. Zhang, R. Polski, A. Thomson, É. Lantagne-Hurtubise, C. Lewandowski, H. Zhou, K. Watanabe, T. Taniguchi, J. Alicea, and S. Nadj-Perge, Nature (London) **613**, 268 (2023).

[11] T. Han, Z. Lu, G. Scuri, J. Sung, J. Wang, T. Han, K. Watanabe, T. Taniguchi, H. Park, and L. Ju, Nat. Nanotechnol. **19**, 181 (2023).

[12] K. Liu, J. Zheng, Y. Sha, B. Lyu, F. Li, Y. Park, Y. Ren, K. Watanabe, T. Taniguchi, J. Jia *et al.*, arXiv:2306.11042.

[13] G. Chen, L. Jiang, S. Wu, B. Lyu, H. Li, B. L. Chittari, K. Watanabe, T. Taniguchi, Z. Shi, J. Jung *et al.*, Nat. Phys. **15**, 237 (2019).

[14] Y.-H. Zhang, D. Mao, Y. Cao, P. Jarillo-Herrero, and T. Senthil, Phys. Rev. B **99**, 075127 (2019).

[15] G. Chen, A. L. Sharpe, E. J. Fox, Y.-H. Zhang, S. Wang, L. Jiang, B. Lyu, H. Li, K. Watanabe, T. Taniguchi *et al.*, Nature (London) **579**, 56 (2020).

[16] A. Abouelkomsan, Z. Liu, and E. J. Bergholtz, Phys. Rev. Lett. **124**, 106803 (2020).

[17] P. J. Ledwith, G. Tarnopolsky, E. Khalaf, and A. Vishwanath, Phys. Rev. Res. **2**, 023237 (2020).

[18] C. Repellin and T. Senthil, Phys. Rev. Res. **2**, 023238 (2020).
[19] P. Wilhelm, T. C. Lang, and A. M. Läuchli, Phys. Rev. B **103**, 125406 (2021).
[20] Y. Xie, A. T. Pierce, J. M. Park, D. E. Parker, E. Khalaf, P. Ledwith, Y. Cao, S. H. Lee, S. Chen, P. R. Forrester *et al.*, Nature (London) **600**, 439 (2021).
[21] F. Wu, T. Lovorn, E. Tutuc, I. Martin, and A. H. MacDonald, Phys. Rev. Lett. **122**, 086402 (2019).
[22] H. Yu, M. Chen, and W. Yao, Natl. Sci. Rev. **7**, 12 (2020).
[23] T. Devakul, V. Crépel, Y. Zhang, and L. Fu, Nat. Commun. **12**, 6730 (2021).
[24] H. Li, U. Kumar, K. Sun, and S.-Z. Lin, Phys. Rev. Res. **3**, L032070 (2021).
[25] V. Crépel and L. Fu, Phys. Rev. B **107**, L201109 (2023).
[26] C. Wang, X.-W. Zhang, X. Liu, Y. He, X. Xu, Y. Ran, T. Cao, and D. Xiao, Phys. Rev. Lett. **132**, 036501 (2024).
[27] A. P. Reddy, F. Alsallom, Y. Zhang, T. Devakul, and L. Fu, Phys. Rev. B **108**, 085117 (2023).
[28] K. Sun, Z. Gu, H. Katsura, and S. D. Sarma, Phys. Rev. Lett. **106**, 236803 (2011).
[29] D. Sheng, Z.-C. Gu, K. Sun, and L. Sheng, Nat. Commun. **2**, 389 (2011).
[30] T. Neupert, L. Santos, C. Chamon, and C. Mudry, Phys. Rev. Lett. **106**, 236804 (2011).
[31] Y.-F. Wang, Z.-C. Gu, C.-D. Gong, and D. N. Sheng, Phys. Rev. Lett. **107**, 146803 (2011).
[32] E. Tang, J.-W. Mei, and X.-G. Wen, Phys. Rev. Lett. **106**, 236802 (2011).
[33] N. Regnault and B. A. Bernevig, Phys. Rev. X **1**, 021014 (2011).
[34] T. Neupert, L. Santos, S. Ryu, C. Chamon, and C. Mudry, Phys. Rev. B **84**, 165107 (2011).
[35] E. J. Bergholtz and Z. Liu, Int. J. Mod. Phys. B **27**, 1330017 (2013).
[36] S. A. Parameswaran, R. Roy, and S. L. Sondhi, C.R. Phys. **14**, 816 (2013).
[37] See Supplemental Material at http://link.aps.org/supplemental/10.1103/PhysRevLett.133.206502, which includes Refs. [38–42], for additional information regarding model parameters, methodologies, ED data on other fractional fillings and spin physics, Hartree-Fock results in the absence of moiré potential and for R4G/*h*-BN and R6G/*h*-BN.
[38] F. Zhang, B. Sahu, H. Min, and A. H. MacDonald, Phys. Rev. B **82**, 035409 (2010).
[39] Y. Park, Y. Kim, B. L. Chittari, and J. Jung, Phys. Rev. B **108**, 155406 (2023).
[40] J. Jung, A. M. DaSilva, A. H. MacDonald, and S. Adam, Nat. Commun. **6**, 6308 (2015).
[41] J. Jung, A. Raoux, Z. Qiao, and A. H. MacDonald, Phys. Rev. B **89**, 205414 (2014).
[42] A. S. Patri and T. Senthil, Phys. Rev. B **107**, 165122 (2023).
[43] R. Roy, Phys. Rev. B **90**, 165139 (2014).
[44] P. J. Ledwith, A. Vishwanath, and D. E. Parker, Phys. Rev. B **108**, 205144 (2023).
[45] N. Bultinck, S. Chatterjee, and M. P. Zaletel, Phys. Rev. Lett. **124**, 166601 (2020).
[46] Y.-H. Zhang, D. Mao, and T. Senthil, Phys. Rev. Res. **1**, 033126 (2019).
[47] C. Repellin, Z. Dong, Y.-H. Zhang, and T. Senthil, Phys. Rev. Lett. **124**, 187601 (2020).
[48] A. L. Sharpe, E. J. Fox, A. W. Barnard, J. Finney, K. Watanabe, T. Taniguchi, M. Kastner, and D. Goldhaber-Gordon, Science **365**, 605 (2019).
[49] M. Serlin, C. Tschirhart, H. Polshyn, Y. Zhang, J. Zhu, K. Watanabe, T. Taniguchi, L. Balents, and A. Young, Science **367**, 900 (2020).
[50] S. Chen, M. He, Y.-H. Zhang, V. Hsieh, Z. Fei, K. Watanabe, T. Taniguchi, D. H. Cobden, X. Xu, C. R. Dean *et al.*, Nat. Phys. **17**, 374 (2021).
[51] H. Polshyn, J. Zhu, M. Kumar, Y. Zhang, F. Yang, C. Tschirhart, M. Serlin, K. Watanabe, T. Taniguchi, A. MacDonald *et al.*, Nature (London) **588**, 66 (2020).
[52] A. Sterdyniak, N. Regnault, and B. A. Bernevig, Phys. Rev. Lett. **106**, 100405 (2011).
[53] B. Zhou, H. Yang, and Y.-H. Zhang, this issue, Phys. Rev. Lett. **133**, 206504 (2024).
[54] J. Dong, T. Wang, T. Wang, T. Soejima, M. P. Zaletel, A. Vishwanath, and D. E. Parker, following Letter, Phys. Rev. Lett. **133**, 206503 (2024).
[55] Z. Tesanovic, F. Axel, and B. I. Halperin, Phys. Rev. B **39**, 8525 (1989).
[56] Z. Dong, A. S. Patri, and T. Senthil, arXiv:2403.07873.
[57] T. Soejima, J. Dong, T. Wang, T. Wang, M. P. Zaletel, A. Vishwanath, and D. E. Parker, companion paper, Phys. Rev. B **110**, 205124 (2024).